Volume 61
Number 72
16 September 2025
Pages 13491–13732

ChemComm

Chemical Communications

rsc.li/chemcomm

ISSN 1359-7345

ROYAL SOCIETY OF CHEMISTRY

FEATURE ARTICLE

Yichi Zhang and Judith Su

FLOWER: a frequency-locked optical whispering evanescent resonator for label-free molecular detection

ChemComm

FEATURE ARTICLE

View Article Online
View Journal | View Issue

Check for updates

Cite this: *Chem. Commun.*, 2025, **61**, 13561

FLOWER: a frequency-locked optical whispering evanescent resonator for label-free molecular detection

Yichi Zhang and Judith Su *

The ability to detect trace amounts of biomolecules, chemicals, and environmental contaminants is critical for advancing diagnostics, drug discovery, and public health. Most high-sensitivity detection methods rely on molecular labels, such as radioactive or fluorescent tags which can perturb the system or may not be feasible in all contexts. In contrast, optical microcavities provide a powerful platform for label-free sensing by confining light and enhancing light-matter interactions. FLOWER (frequency locked optical whispering evanescent resonator) is a versatile sensing technique that can be applied to any optical microcavity to enable real-time, quantitative detection with high sensitivity and stability. In our work, we pair FLOWER with silica microtoroid resonators that offer ultra-high quality factors for prolonged light confinement, along with a small footprint and compatibility with on-chip fabrication. By combining these features, FLOWER bridges the gap between high performance and portability, making it particularly well suited for precision sensing. FLOWER has enabled label-free detection at the single-molecule and zeptomolar levels. In this review, we place FLOWER within the broader optical sensing landscape, highlighting how it addresses longstanding challenges in sensitivity, noise suppression, and molecular specificity across a wide range of chemical and biological applications.

Received 17th June 2025,
Accepted 1st August 2025

DOI: 10.1039/d5cc03427b

rsc.li/chemcomm

Published on 11 August 2025. Downloaded on 9/5/2025 5:21:07 PM.

Microtoroid resonators

Microresonators, such as microtoroids, possess unique optical properties due to their support of whispering gallery modes (WGMs), resonant modes in which light circulates along the perimeter of the structure through total internal reflection.[1] The concept of whispering gallery modes originates from the acoustic phenomenon first described by Lord Rayleigh in 1878,[2,3] who observed that sound waves could propagate efficiently along curved walls, such as the gallery beneath the dome

1630 E. University Blvd, Tucson, AZ, USA. E-mail: judy@optics.arizona.edu

Yichi Zhang

Yichi Zhang is a PhD student in the Wyant College of Optical Sciences at the University of Arizona. He received his BS degree in Physics from Shandong University, with research experience in astronomy and condensed matter physics. His current research focuses on high-resolution optical sensing and whispering gallery mode resonators.

Judith Su

Judith Su is a Craig M. Berge Faculty Fellow and an Associate Professor of Biomedical Engineering and Optical Sciences at the University of Arizona. She received her BS and MS from MIT in Mechanical Engineering and her PhD from Caltech in Biochemistry and Molecular Biophysics. Her research focuses on developing ultrasensitive optical sensors for applications in biology, medicine, and environmental monitoring. She is a recipient of the NSF CAREER Award, NIH R35 MIRA, and several early career honors. She is a Fellow of SPIE, and served as general chair for Opticas Integrated Photonics Research Conference in 2023, 2024, and 2025.

Published on 11 August 2025. Downloaded on 9/5/2025 5:21:07 PM.

of St. Paul's Cathedral. This analogy was later extended to optics, where light travels similarly along the interior boundaries of dielectric resonators with minimal loss.[4]

In optical WGMs, light confinement leads to long photon lifetimes and evanescent fields that extend beyond the resonator surface, enabling interaction with the surrounding environment. However, not all WGM resonators exhibit large evanescent fields—some, such as certain high-Q microdisks, achieve low loss by tightly confining light away from the surface. In contrast, microtoroids not only support ultra-high-Q WGMs but also feature significant ($\sim$100 nm in length) evanescent fields, making them particularly suitable for sensing applications.[5,6]

Microtoroids were first invented in 2003.[7] Their fabrication process begins with steps commonly used for silica microdisks, namely photolithography, wet oxide etching, and dry silicon etching; however, the toroid fabrication process has an additional key thermal reflow step that is performed using a CO_2 laser. During this reflow step, the edge of the silica microdisk melts and reshapes to a smooth toroidal geometry,[1,8] as shown in Fig. 1. This polishing step dramatically reduces surface roughness and thus scattering loss, enabling ultra-high quality factor (Q) factors in excess of 100 million to be obtained.

Microdisks and microrings have also demonstrated high Q performance;[9–11] however, microtoroids are particularly well suited for precision sensing due to their unique combination of ultra-high Q, large evanescent field, and compatibility with on-chip fabrication.[5] The high Q-factor indicates low intrinsic losses such as absorption, radiation, and scattering, allowing light to circulate many times within the resonator. In comparison, achieving a similar Q-factor with a microring would require a diameter of 23.6 mm, making microtoroids significantly more space-efficient for multiplexing applications. This extended light confinement enhances light-matter interactions, enabling the detection of small perturbations, including those of single molecules.[12,13]

Although microtoroids offer an ideal platform for high-sensitivity sensing due to their ultrahigh Q and strong light-matter interactions, the detection method itself plays a critical role in determining overall performance. In this context, FLOWER[14,15] represents a significant departure from previous microtoroid-based biosensing approaches. We note that FLOWER is distinct from the single-molecule microtoroid biosensing work of Armani *et al.*,[16] which has not been independently reproduced. Unlike the passive wavelength-shift detection method employed in that work, FLOWER uses active frequency locking, balanced detection, and data processing to enable robust measurements. This difference enables reliable and quantitative detection at both single-molecule and zeptomolar concentrations.

Toroids have since been widely used in biosensing,[5,17–24] environmental monitoring,[25,26] and fundamental studies in cavity quantum electrodynamics.[27] Ongoing efforts to further enhance their performance include plasmonic coupling[28] and optical frequency comb generation.[29,30] These efforts are expanding the capabilities of microtoroids and FLOWER as next-generation optical sensors.

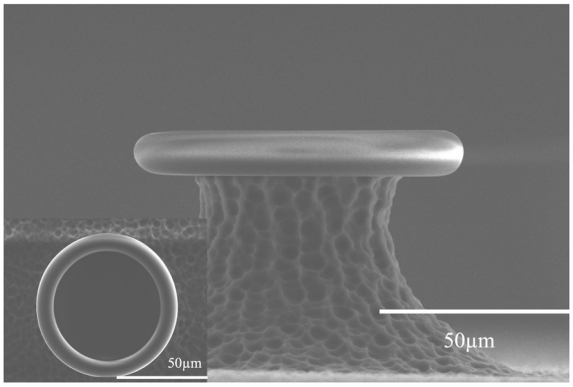

Fig. 1 SEM image of a silica microtoroid (side view). The microtoroid, formed by reflowing a silica microdisk, is supported by a silicon pillar. The inset shows a top-view SEM image of the microtoroid.

FLOWER system

FLOWER is an optical sensing technique that leverages microcavities for high sensitivity, label-free detection. Its core sensing element is an optical microcavity, such as a silica microtoroid. When light is evanescently coupled into the resonator, it circulates along the periphery *via* total internal reflection. Resonance occurs when the round-trip optical path length is an integer multiple of the wavelength, leading to constructive interference. This resonance condition enables strong field buildup and mode enhancement within the microtoroid, amplifying light-matter interactions critical for sensing. This resonant behavior produces a characteristic Lorentzian lineshape in the transmission spectrum, given by:

$$T = \left(\frac{\tau_{ext} - \tau_{int} - i\Delta\omega}{\tau_{ext} + \tau_{int} + i\Delta\omega}\right)^2 \quad (1)$$

where $\Delta\omega = \omega_0 - \omega$, with ω_0 denoting the resonance frequency and ω the input laser frequency. The intrinsic lifetime, τ_{int}, characterizes the inherent losses of the optical resonator, while τ_{ext} describes the coupling losses to the external waveguide.[31–33]

The total quality factor Q of a fiber-coupled microtoroid can be expressed in terms of the intrinsic lifetime τ_{int} and the external coupling lifetime τ_{ext}, given by:[8,31]

$$Q_{tot} = \omega_0 \tau_{tot} \quad (2)$$

$$\frac{1}{\tau_{tot}} = \frac{1}{\tau_{int}} + \frac{1}{\tau_{ext}} \quad (3)$$

Molecular binding events are detected through resonance frequency shifts of the toroid, which can be described by the Bethe–Schwinger cavity perturbation formula.[34] To monitor these shifts in sensing experiments, the laser wavelength is typically scanned to obtain the transmission spectrum. In FLOWER the laser is actively locked to the cavity's resonance (Fig. 2). This enables smaller and more transient events to be measured. A frequency-modulated dither signal is applied and mixed with the photodetector output, producing an error signal.[35] This error signal, which is proportional

 This journal is © The Royal Society of Chemistry 2025

Published on 11 August 2025. Downloaded on 9/5/2025 5:21:07 PM.

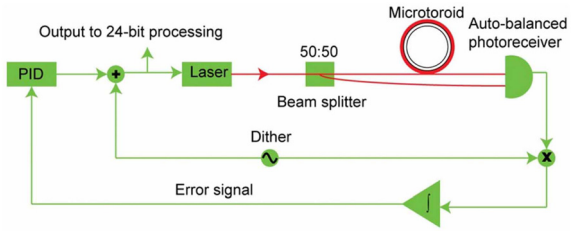

Fig. 2 Block diagram of the FLOWER system. A frequency-modulated laser generates a signal that, when mixed with a dither signal, produces an anti-symmetric error signal. The error signal is processed by a proportional-integral-derivative (PID) controller, which dynamically adjusts the laser frequency to maintain resonance stability. Reproduced from ref. 20 with permission from the American Chemical Society, copyright 2015.

to the frequency offset between the laser and the resonant mode, has an antisymmetric shape around resonance that enables sensitive and directional tracking of frequency shifts, offering improved performance over conventional side-locking techniques. A feedback loop incorporating a PID controller continuously adjusts the laser frequency based on this error signal. This adaptive locking mechanism ensures that the laser remains locked to a specific resonance mode of the microtoroid, enabling real-time tracking of the resonance frequency and reducing the minimum detectable time interval to $\sim$1 ms.[20,36–39]

Biochemical sensing

FLOWER-based microtoroid sensing (Fig. 3(a)) has emerged as a leading label-free sensing technology,[40] due in part to the microtoroids ability to confine light for extended periods, which enhances evanescent field interactions at the sensor interface. Compared to alternative bare resonator geometries such as microspheres[39] and microdisks,[10,11] as well as plasmonic platforms like surface plasmon resonance (SPR) and localized SPR (LSPR) sensors,[41,42] microtoroids integrated with FLOWER offer highly stable detection down to the single-molecule level for analytes just a few nanometers in size.[5,43] While LSPR has also achieved single-molecule sensitivity, it is often limited by signal variability. In contrast, FLOWER enables reliable quantification of trace analytes in complex environments, making it broadly applicable to biochemical sensing, environmental monitoring, and medical diagnostics. In parallel, nanopore-based techniques have recently demonstrated the ability to resolve fine structural differences in hydrogen bonding[44] and enable single-molecule discrimination of biomolecules through ion dependent tuning,[45] further highlighting the growing toolbox of label-free single-molecule biosensing platforms. FLOWER contributes to this progress by offering a stable and reproducible optical alternative that enables reliable quantification of trace analytes in complex environments, making it broadly applicable to biochemical sensing, environmental monitoring, and medical diagnostics.

The single-molecule detection capabilities of the FLOWER system in aqueous solution were first demonstrated in a 2014 doctoral dissertation[12] and later published in Su *et al.*[5] These

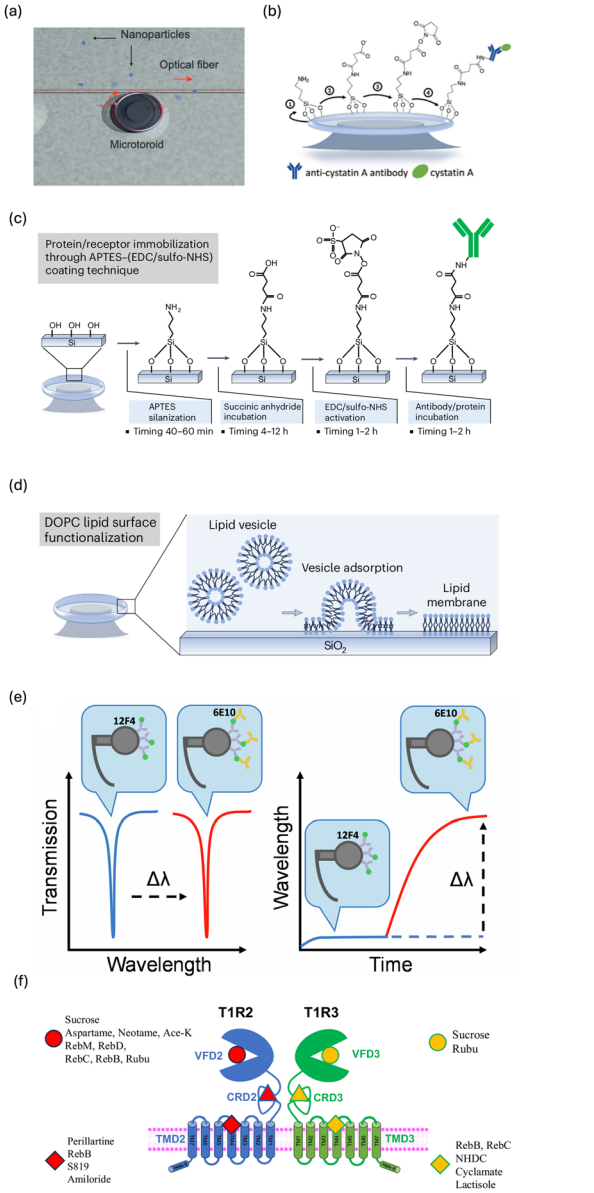

Fig. 3 FLOWER system biosensing schematic. (a) When a frequency-locked tunable laser is coupled into the microtoroid *via* an optical tapered fiber, the light is continuously confined within the microtoroid rim. This confinement produces an extended evanescent wave that polarizes nearby nanoparticles. Changes in the resonant wavelength resulting from the polarization of these particles are then used to detect the presence of various bioparticles. Reproduced with permission from ref. 5. Copyright © 2016, The Author(s), licensed under CC BY 4.0. (b) Functionalization steps and incubation of cystatin A on the microtoroid. Reproduced with permission from ref. 46. © 2023 Elsevier on behalf of ASBMB. (c) The protein/receptor immobilization process consists of APTES silanization, succinic anhydride incubation, EDC/sulfo-NHS activation, and subsequent antibody/protein incubation. Reproduced with permission from ref. 40. Copyright © 2025, Springer Nature Limited. (d) DOPC lipid surface functionalization occurs as DOPC vesicles adsorb onto SiO_2, rupture, and form a supported lipid bilayer on the microtoroid surface. Reproduced with permission from ref. 40. Copyright © 2025, Springer Nature Limited. (e) The 12F4 clone antibody, specific to β-Amyloid 1-42, is functionalized onto the toroid surface. Upon binding of the 6E10 clone antibody, which targets β-Amyloid 1–16, the binding mechanism induces a resonant wavelength shift due to the interaction between 6E10 and 12F4. Reproduced with permission from ref. 19.© 2024, The Author(s), licensed under CC BY 4.0. (f) The T1R2/T1R3 Human heterodimeric sweet taste receptor binds sweet ligands at multiple sites. Reproduced with permission from ref. 18.© 2024, The Author(s), licensed under CC BY 4.0.

Published on 11 August 2025. Downloaded on 9/5/2025 5:21:07 PM.

studies showed that FLOWER can detect a wide range of individual biomolecular targets—including exosomes from human mesenchymal stem cells, yeast ribosomes, mouse immunoglobulin G, and human interleukin-2—spanning particle radii from approximately 45 nm down to less than 2.5 nm (corresponding to a molecular weight of 15.5 kDa).[5] By applying a step-finding algorithm developed by Kerssemakers *et al.*,[47] FLOWER was able to resolve discrete, step-like binding events, with amplitudes that depend on both the particle's polarizability and its binding location on the toroid. The observed exponential distribution of dwell times suggests that adsorption follows Poisson statistics, consistent with independent, stochastic binding events. To estimate the molecular mass of individual analytes, the maximum step amplitude in the binding histogram was used.

To enable selective detection, the silica surface of the microtoroid is functionalized with molecular recognition elements. This allows FLOWER to detect a wide variety of targets, including exosomes,[20] ligands binding to human taste receptors (both sweet and bitter),[18] proteins associated with neurodegenerative diseases,[19] membrane receptor interactions,[17] and small-molecule drugs that bind to the receptor-binding domain (RBD) of SARS-CoV-2 to block its interaction with the human ACE2 receptor.[21] Typically, proteins or receptors are immobilized on the microtoroid surface *via* covalent bonding. As illustrated in Fig. 3(b) and (c), the process begins with surface functionalization using APTES silane in acetic acid, which introduces amine groups. The chip is then succinylated with succinic anhydride in dimethylformamide and activated with EDC/sulfo-NHS in MES buffer, generating reactive carboxyl groups. These groups form stable amide bonds with primary amines on the target protein or receptor during incubation, enabling covalent immobilization.[40] As shown in Fig. 3(d), an alternative approach involves coating the microtoroid with a DOPC lipid bilayer. This is achieved by first forming a thin lipid film from chloroform-dissolved DOPC, followed by rehydration in buffer to produce unilamellar vesicles. These vesicles then fuse spontaneously onto the cleaned microtoroid surface, forming a continuous membrane. Once functionalized, the microtoroid can be used for specific bioparticle incubation.

Utilizing these selective detection approaches, FLOWER has been used for cancer diagnostics. For example, Luu *et al.*[46] used FLOWER to detect human cystatin A Fig. 3(b), a cysteine proteinase inhibitor and promising biomarker for ovarian cancer, at picomolar concentrations corresponding to its levels in murine vaginal lavage samples. FLOWER exhibited lower detection thresholds compared to conventional techniques such as MALDI-TOF MS Notably, it was able to distinguish between healthy individuals and ovarian cancer patients using human tampon-derived samples, highlighting its potential as a non-invasive diagnostic tool.

In addition to cancer diagnostics, FLOWER has also been used to detect neurodegenerative diseases. Specifically, FLOWER was used to detect amyloid beta 1–42 (Aβ42) in postmortem cerebrospinal fluid using a surface-immobilized Aβ-specific antibody. The binding-induced resonance shift, illustrated in Fig. 3(e), resulted in an area under the ROC curve (AUC) of 0.92, surpassing that of a standard ELISA kit (AUC = 0.82) for Alzheimer's disease diagnosis.[19,48] FLOWER successfully distinguished between control patients, those with mild cognitive impairment (MCI), and individuals with Alzheimer's disease (AD), demonstrating its potential for disease stratification. It enabled detection of Aβ42 at picomolar concentrations, consistent with its physiological levels in cerebrospinal fluid, as also reported by advanced label-free nanopore sensors.[49] Beyond diagnostics, FLOWER has been applied to receptor–ligand interaction studies. As shown in Fig. 3(f), it was used to investigate ligand binding to the human heterodimeric taste receptor T1R2/T1R3, providing insight into the molecular recognition of sweet and bitter compounds.[18,50]

FLOWER has also been employed to study extracellular vesicles and membrane-associated targets, expanding its utility to cancer monitoring, drug discovery, and mechanistic studies of toxin and receptor interactions. Exosomes are increasingly recognized as critical mediators of intercellular communication in cancer biology, originating from both cancer cells and supporting components within the tumor microenvironment.[22] FLOWER offers a label-free method for detecting nanoscale bioparticles in aqueous environments and was the first technique to detect single exosomes. In one study, diluted mouse serum from animals implanted with human Burkitt's lymphoma tumor cells was flowed over a microtoroid covalently functionalized with anti-CD81, an exosome-specific surface marker.[20,51,52] When exosomes bind to the microtoroid, the effective optical path length increases as light couples into the vesicles, producing a detectable resonance wavelength shift. The amplitude of this shift correlates with tumor progression in the mice, enabling a minimally invasive method for tumor monitoring and early disease detection across a range of biological samples.

In the context of drug discovery and toxicity screening, FLOWER provides label-free, rapid,[53] and highly sensitive detection. This capability streamlines experimental workflows and increases the likelihood of identifying biomolecular interactions that might be missed by conventional labeling techniques. For instance, FLOWER has been used to detect cholera toxin B using microtoroids functionalized with DOPC lipid bilayers doped with GM1 receptors. In another application, κ-opioid receptors (κORs) were reconstituted into a supported lipid bilayer on the microtoroid surface through micelle dilution. In this approach, detergent-solubilized κOR micelles are mixed with phospholipids, and as the detergent is gradually diluted below the critical micelle concentration, the micelles disassemble and the receptors incorporate into the bilayer while preserving their native conformation. This setup enabled real-time analysis of competitive binding between the opioid antagonist naloxone and the endogenous neuropeptide DynA 1–13.[17]

In a small-molecule drug screening study targeting severe acute respiratory syndrome coronavirus 2 (SARS-CoV-2), FLOWER was employed to measure the binding interaction between the viral spike protein receptor-binding domain (Spike-RBD) and human ACE2 (hACE2) receptors immobilized on microtoroids (Fig. 4). To assess the inhibitory effects of

 This journal is © The Royal Society of Chemistry 2025

Published on 11 August 2025. Downloaded on 9/5/2025 5:21:07 PM.

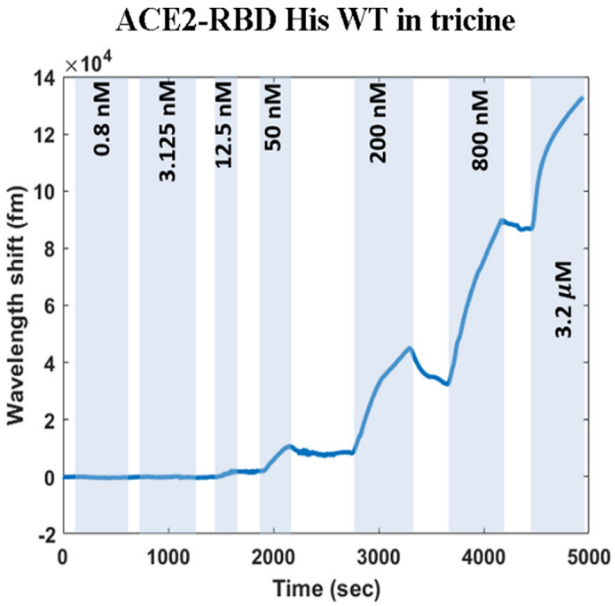

Fig. 4 Wavelength shift of the FLOWER system showing binding of Spike-RBD-His wildtype (WT) to hACE2 in tricine buffer. Blue-shaded regions indicate exposure to increasing concentrations of Spike-RBD, while unshaded regions correspond to running buffer rinses. Reproduced from ref. 21. With permission from the American Chemical Society, copyright 2024.

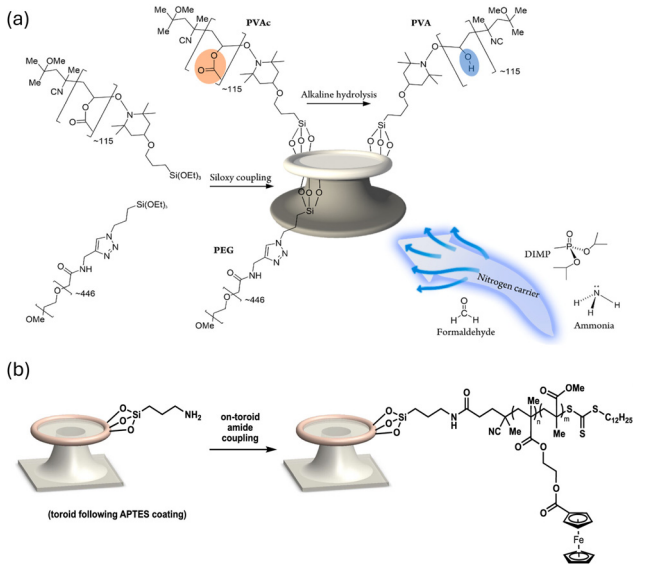

Fig. 5 Gas sensing using FLOWER. (a) Microtoroids are coated with siloxy-terminated polymer films—PEG, PVAc, and PVA—*via* siloxy coupling. Nitrogen-carried analytes such as diisopropyl methylphosphonate (DIMP), formaldehyde, and ammonia are transported to the polymer-coated surface for selective detection. Reproduced from ref. 25 with permission from the American Chemical Society, copyright 2022. (b) A copolymer brush composed of 2-(methacryloyloxy)ferrocenecarboxylate (FcMA) and methyl methacrylate (MMA) is grafted onto the microtoroid surface *via* on-toroid amide coupling following APTES treatment. This selective functionalization enables nitric oxide (NO) detection at parts-per-trillion levels. Reproduced from ref. 26 with permission from the American Chemical Society, copyright 2024.

candidate compounds, each drug was premixed with a set concentration of Spike-RBD before being introduced to the hACE2-functionalized microtoroid. The resulting binding curves were analyzed to evaluate inhibition. Both methotrexate and diethylenetriamine pentaacetic acid (DTPA) significantly reduced Spike-RBD binding to hACE2, suggesting their potential to block viral entry into host cells.[21]

Environmental monitoring

Beyond biosensing, FLOWER can also be adapted for gas sensing by applying polymer layers designed for chemical selectivity.[25,26] In a study by Li *et al.*,[25] microtoroids were coated with various siloxy-terminated polymer films using siloxy coupling, as shown in Fig. 5(a). The polymers, (3-triethoxysilyl)propyl-terminated polyethylene glycol (PEG), polyvinyl acetate (PVAc), and polyvinyl alcohol (PVA), were synthesized through amidation using (3-aminopropyl)triethoxysilane (APTES) to allow efficient conjugation to the silica surface.[54] These polymer-coated microtoroids were used to detect nitrogen-carried vapors of the chemical warfare agent surrogate diisopropyl methylphosphonate (DIMP), as well as toxic industrial chemicals such as formaldehyde and ammonia, at parts-per-trillion concentrations. Each polymer coating induced a distinct resonance wavelength shift in the microtoroid sensor upon exposure to its target analyte. A mixture of PEG and PVAc enabled reliable detection of both DIMP and ammonia at part-per-trillion concentrations as well.[25]

One advantage of the FLOWER system for gas sensing, compared to other ultra-sensitive sensors such as those based on single-walled carbon nanotubes,[55] pristine graphene,[56,57] and pristine carbon nanotubes,[58] lies in its ability to achieve part-per-trillion detection limits while maintaining high analyte selectivity. Xu *et al.*[26] demonstrated that FLOWER can detect nitric oxide (NO) at low part-per-trillion concentrations (Fig. 6). This selectivity arises from the specific binding of NO to iron (Fe) centers in copolymers composed of 2-(methacryloyloxy)ferrocenecarboxylate (FcMA) and methyl methacrylate (MMA). These copolymers are applied as a polymer brush on the microtoroid surface through amide coupling, using 3-(aminopropyl)triethoxysilane (APTES) for surface functionalization,[26] as shown in Fig. 5(b). In addition, FLOWER maintains its sensitivity to NO even under high humidity, highlighting its robustness for real-world environmental monitoring.

Next generation sensing platforms

Surface-functionalized microtoroid sensors are typically limited to detecting particles that bind specifically to the functional groups attached to their surfaces. One strategy to expand the range of detectable analytes is to leverage the intrinsic spectroscopic properties of the microtoroid itself.[39,59,60] Choi *et al.* demonstrated the first optical frequency combs generated in an aqueous environment, marking a significant advance in microresonator based spectroscopy.[30] These combs were produced using microtoroid resonators, highlighting their potential for future sensing applications in liquid-phase systems. Guided by near-visible wavelength simulations of dark soliton generation driven by avoided mode crossings (AMX),[29] the study identified strong AMX effects and, in some cases, competition between

Published on 11 August 2025. Downloaded on 9/5/2025 5:21:07 PM.

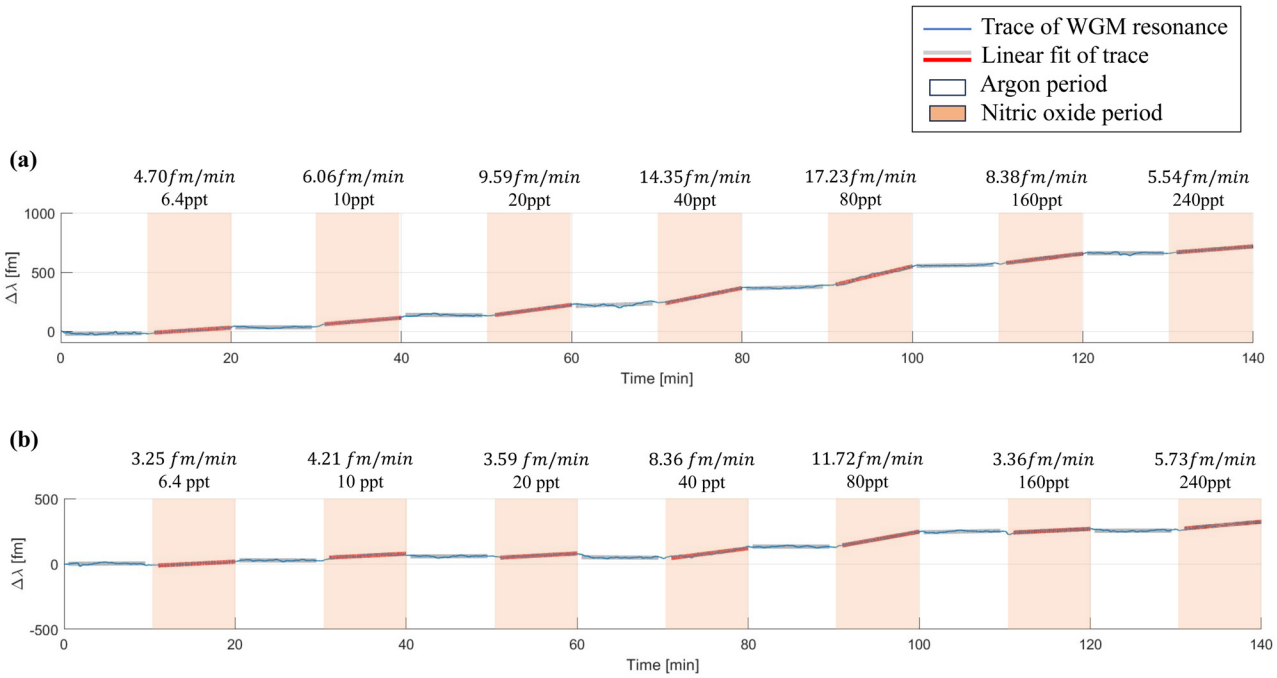

Fig. 6 Detection of nitric oxide using FLOWER sensors with FcMA/MMA copolymers of varying compositions. (a) Higher FcMA content; (b) higher MMA content. Shaded regions indicate nitric oxide exposure; unshaded regions denote argon. Reproduced from ref. 26 with permission from the American Chemical Society, copyright 2024.

AMX features as key mechanisms underlying primary comb formation. As illustrated in Fig. 7, the integrated dispersion plots reveal normal dispersion across the mode families, with the primary comb (highlighted in green) forming at the AMX wavelength. Rather than relying on conventional frequency locking with a PID-controlled error signal, the system employs a self-stabilizing thermal locking technique to maintain resonance.[61] Larger microtoroids (~500 μm diameter) were

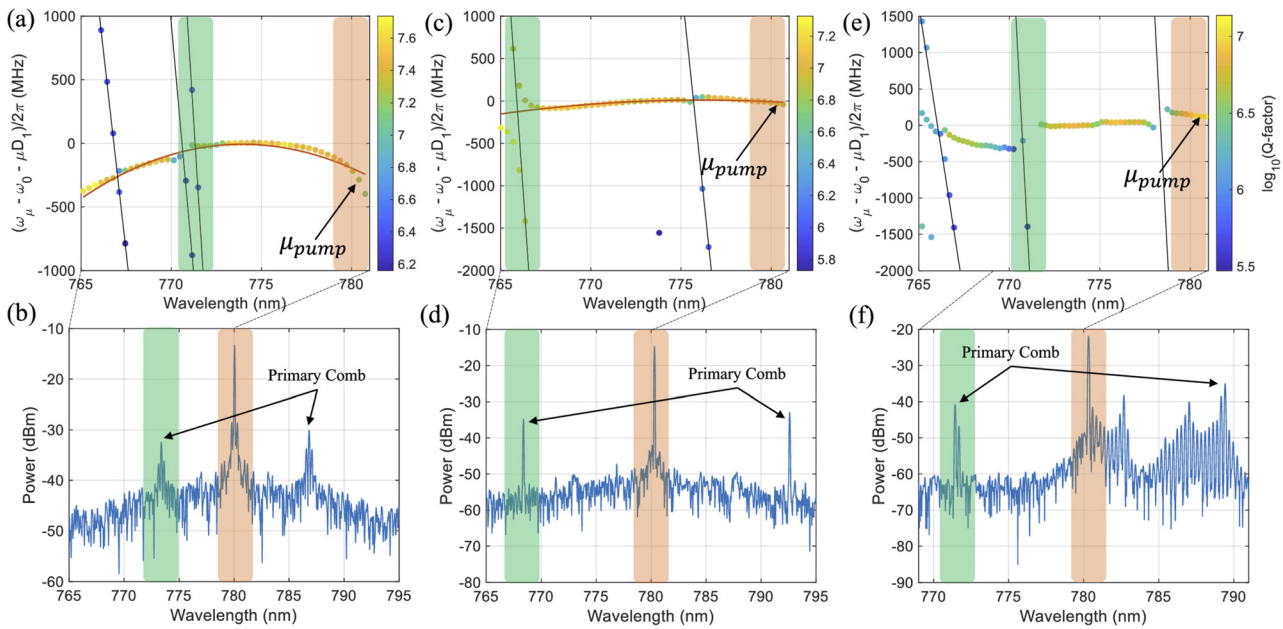

Fig. 7 Integrated dispersion diagram for frequency comb generation in an aqueous environment. Panels (a), (c), and (e) show the integrated dispersion of three different mode families, each exhibiting normal dispersion. Avoided mode crossings (AMXs) are highlighted in green, and the pump wavelengths are marked in orange. Panels (b), (d), and (f) show the corresponding optical spectra of frequency combs generated in water. In each case, the primary comb, highlighted in green, emerges at the wavelength where the AMX occurs, while the pump wavelength is indicated in orange. Reproduced from ref. 30 with permission from Optica, copyright 2022.

 This journal is © The Royal Society of Chemistry 2025

Published on 11 August 2025. Downloaded on 9/5/2025 5:21:07 PM.

used to observe more avoided mode crossings (AMX), as their smaller free spectral range (FSR) leads to a denser mode spacing and more frequent mode interactions. In the future, artificial intelligence (AI) techniques, including machine learning and deep learning, can enable the identification, classification, and prediction in real time of spectral fingerprints generated by optical frequency combs for various chemical components in gases and aqueous solutions. Models such as CNN[62–64] and PLS-DA[65] show great potential for integrating microtoroid-generated frequency combs with AI for real-time biosensing, environmental monitoring, and disease diagnosis.

Microtoroid resonators can also be used for photothermal microscopy, as their resonance wavelength changes in response to localized heating.[66] FLOWER predates[12,20,67] a frequency-locked photothermal variant later demonstrated by Heylman *et al.* using a similar setup.[68] Although single-molecule sensitivity was claimed, the approach did not demonstrate it experimentally, in part due to limitations in tracking resonance shifts using the error signal at high modulation frequencies. By contrast, our method monitors the PID controller output at lower modulation frequencies, enabling more accurate tracking and significantly improved sensitivity. As demonstrated by Hao *et al.*,[69] the FLOWER system, combined with an amplitude modulated (AM) 405 nm pump laser (Fig. 8(a)), can detect heat dissipation from particles on the microtoroid surface. When frequency locked to resonance, the system isolates the modulated thermal signal using a lock-in amplifier. By scanning the pump laser in two dimensions with a galvo mirror and monitoring the resulting resonance shifts, precise locations of individual particles can be determined. Using a re-etched microtoroid with a smaller pillar to minimize background noise, the FLOWER system enables detection of single quantum dots (QDs) as small as 5 nm in diameter, with a signal-to-noise ratio exceeding 10^4. This technique offers the potential for highly sensitive detection of biological structures[70,71] and outperforms fluorescence-based methods for non-luminescent particle detection.[39,72]

For enhanced sensitivity, the bare microtoroid FLOWER system can be coupled with plasmonic nanoparticles, such as gold nanorods, which amplify the evanescent field through localized surface plasmon resonance (LSPR) effects.[74] According to perturbation theory,[75] the resonance wavelength shift depends on the spatial overlap between the perturbation and the intensity of the evanescent electric field of the whispering-gallery modes (WGM) of the microtoroid, normalized by the total energy stored in the cavity. Therefore, local plasmonic enhancement, such as the intensified electric field at the hotspot of a plasmonic nanoparticle, can significantly increase sensitivity.

Li *et al.* used a 3D eigenmode simulation to analyze a complete microtoroid (10 μm major diameter) coupled to a gold nanorod, with a nearby nanosphere representing an analyte molecule in the near field[28] (Fig. 8(b)). To quantify the effect of localized surface plasmon resonance (LSPR) on the system, a combined enhancement factor, f_C, was defined which captures the trade-off between optical field enhancement from plasmonic coupling and the degradation of the quality factor (Q) due to

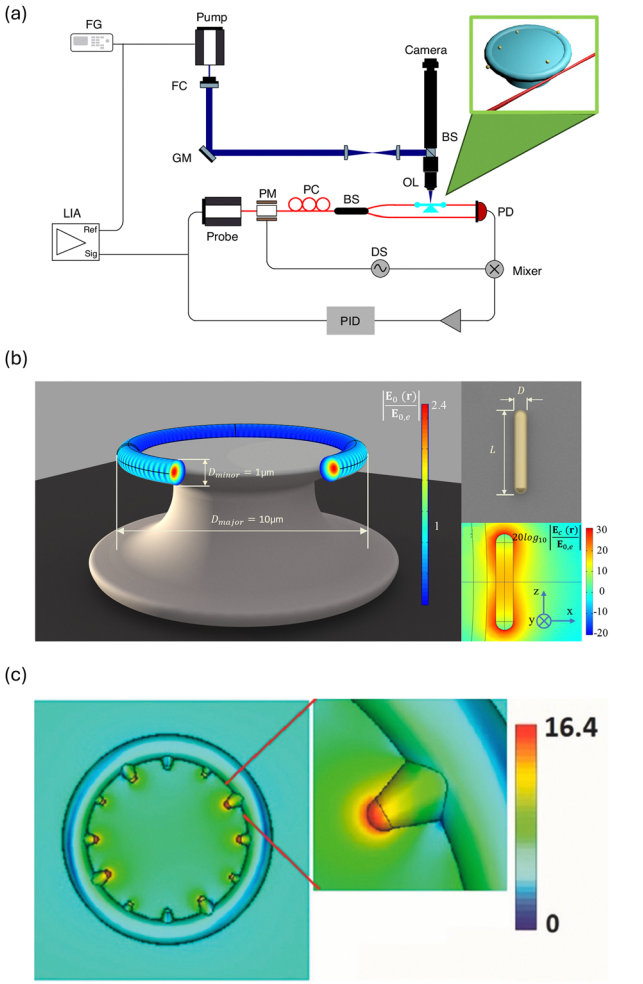

Fig. 8 Next-generation sensing platforms. (a) Schematic of a photothermal spectroscopy system. An amplitude-modulated (AM) 405 nm pump laser is steered by a galvo mirror to perform 2D scanning across the microtoroid surface. The FLOWER system, combined with a lock-in amplifier (LIA), extracts the photothermal signal in real time. Reproduced from ref. 69. Copyright © 2024, The Author(s). (b) Left: 3D eigenmode simulation of a microtoroid with a 10 μm major diameter, showing the normalized evanescent electric field amplitude along its rim. Right upper: simulation of a gold nanorod with length L and diameter D; right lower: electric field distribution of the excited dipole mode surrounding the nanorod. Reprinted with permission from ref. 28. Copyright Optical Society of America. (c) Simulated normalized electric field distribution of 780 nm light incident on toroidal gold particles (tAUPs) with spikes. The inset highlights the strong localized field at a plasmonic hotspot. Reproduced from ref. 73 with permission from the American Chemical Society, copyright 2019.

additional scattering and absorption losses. These findings suggest that optimal performance is achieved with slight detuning between the WGM and the plasmonic resonance, which maintains a relatively high Q while still providing significant intensity enhancement.

Arranging three gold nanorods into a plasmonic trimer enables the excitation of dark modes, which reduce radiative losses compared to those in single nanorod systems. Simulations show that this trimer configuration can achieve a combined enhancement factor (f_C of approximately 105 (with a rod

Published on 11 August 2025. Downloaded on 9/5/2025 5:21:07 PM.

aspect ratio of 4.5), notably higher than the f_C of about 84 observed for a single nanorod with an aspect ratio of 5. In addition to greater field enhancement, the trimer offers improved robustness to orientation variations, making it a promising candidate for ultra-sensitive biosensing applications.[28] Such plasmonic trimers can also be introduced and positioned using optical tweezers.[76,77]

Raman spectroscopy is another biosensing approach, where incident light interacts with molecular vibrations, resulting in a characteristic scattering spectrum that reveals molecular composition.[78] Nguyen *et al.* demonstrated that spiked toroidal gold particles (tAUPs), shown in Fig. 8(c), exhibit high surface-enhanced Raman scattering (SERS) sensitivity for detecting 4-mercaptobenzoic acid (4-MBA).[73] A one-step synthesis method, based on the use of mixed counterionic surfactants (sodium dodecyl sulfate, SDS, and cetyltrimethylammonium bromide, CTAB) and temperature control, produced tAUPs in three distinct size and shape variants. The enhancement factors achieved with these tAUPs were approximately two orders of magnitude higher than those of gold nanostars and an order of magnitude higher than nanoflowers.

Free-space coupling for whispering gallery mode biochemical sensors

WGM sensors based on microtoroid resonators have demonstrated exceptional sensitivity in laboratory settings, typically relying on tapered optical fibers for evanescent coupling.[5,20] However, these tapered fibers are highly fragile, particularly in aqueous or mechanically dynamic environments, making them poorly suited for industrial and field applications due to their susceptibility to vibrations and physical strain. To overcome these limitations, free-space coupling has emerged as a more robust alternative, offering improved mechanical stability while preserving high sensitivity.

In a simulation study,[79] a phased array of nanorods was strategically placed along the rim of a microtoroid. Using periodic Floquet-wedge boundary conditions and the beam envelope method solver (FloWBEM), the study simulated traveling WGMs within this nanostructured geometry. The simulations predicted loaded quality (Q) factors up to 2.1×10^7 and signal-to-background ratios as high as 3.86. Suebka *et al.* experimentally demonstrated free-space light coupling to microtoroid resonators.[80] Q's in excess of 10^8 were demonstrated with this approach. As illustrated in Fig. 9, a collimated free-space laser beam is directed onto the microtoroid surface, and the backscattered light is recollimated by the same objective lens. This recollimated signal is captured by a digital micromirror device (DMD), which enables monitoring of the resonance wavelength. The study examined the effect of the Gaussian beam waist on coupling performance by comparing two objective lenses ($\times$ 5 with NA = 0.14 and $\times$ 20 with NA = 0.42). The results revealed a trade-off between the coupling efficiency and the illumination area: smaller beam spots yielded higher coupling efficiency, while larger spots covered broader interaction regions.

A further advantage of this free-space approach is the ability to modulate the phase relationship among interfering cavity modes by adjusting the distance between the laser beam and the resonator. This allows for manipulation of the Fano resonance lineshape, which can enhance the sensitivity of biomedical sensing applications.[81] Additionally, when integrated with FLOWER, this free-space coupling configuration enabled validation of thermal nonlinearities and the development of a temperature sensor, demonstrated by a linear wavelength shift with increasing temperature. These results confirm the mechanical robustness and functional versatility of free-space coupled FLOWER systems and highlight their suitability for deployment in biomedical sensing, environmental monitoring, and other challenging environments where tapered fiber coupling is impractical.

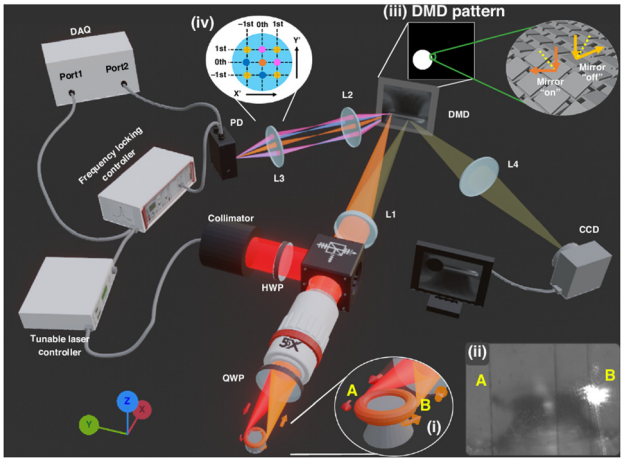

Fig. 9 Free-space coupling system for microtoroid resonance tracking. A 5× objective lens is used to collimate the incident light and the scattered light at 180° from the incident direction. The collimated light is directed to a digital micromirror device (DMD) and then to a photodetector (PD) for resonance wavelength observation. Reproduced with permission from ref. 80. Copyright © 2024, The Author(s).

Future outlook and conclusion

In this article, we focused on FLOWER (frequency-locked optical whispering evanescent resonator), a highly sensitive platform that leverages the ultra-narrow linewidths of high-Q optical resonators to detect minute changes in refractive index. While microtoroids are frequently used due to their exceptionally high Q factors, favorable geometry, biocompatibility, ease of surface functionalization, and compatibility with on-chip fabrication techniques, FLOWER is a generalizable technique that can be implemented across a variety of WGM resonator geometries and materials. We reviewed the fabrication of microtoroid resonators, the physical mechanisms behind their performance, and the frequency-locking strategies that underpin FLOWERs ability to precisely track resonance shifts.

We also explored advances that expand the capabilities of FLOWER-based sensing systems. These include photothermal microscopy, plasmonic enhancement to improve biosensing sensitivity, and the generation of frequency combs in aqueous environments for high-precision optical interrogation, spectroscopic fingerprinting, and potential integration of AI with optical frequency combs for advanced analysis. Importantly,

 This journal is © The Royal Society of Chemistry 2025

Published on 11 August 2025. Downloaded on 9/5/2025 5:21:07 PM.

frequency combs can enable an agnostic sensing platform, where *a priori* knowledge of the target analyte is not required, making it possible to detect and differentiate unknown or emerging compounds based solely on their spectral signatures. Additionally, we discussed nanostructure-enhanced Raman scattering for chemical detection, and emerging methods such as free-space optical coupling, which offer more robust and scalable alternatives to conventional tapered fiber coupling.

FLOWER-based sensors have demonstrated impact in a range of applications, from biosensing and chemical detection to environmental monitoring and optical metrology. Moving forward, the integration of FLOWER with scalable on-chip platform and multiplexing architectures[82] will be key to transitioning these sensors from the laboratory to real-world deployment. Emerging fabrication approaches such as 3D-printed resonator structures,[83,84] while currently limited in achievable *Q*-factors, may offer promising avenues for rapid prototyping or integration with low-cost platforms. Coupling these advances with engineered plasmonic or dielectric nanostructures may further boost sensitivity without compromising *Q*, unlocking the potential for portable and cost-effective super sensors. The integration of FLOWER with quantum photonics, for example, through the use of entangled photons to overcome classical noise limitations, could enable further precision in sensing and expand the frontiers of measurement science. Likewise, combining FLOWER with machine learning and AI-driven analytics offers a pathway to autonomous, adaptive sensing systems capable of extracting meaningful insights from complex or dynamic environments. With continued development, FLOWER holds promise for transformative applications in medicine, environmental science, quantum technologies, AI-enabled diagnostics, and the advancement of fundamental science.

Author contributions

Y. Z drafted the initial version of the manuscript. J. S. provided critical revisions, conceptual guidance, and final editing. Both authors reviewed and approved the final version.

Conflicts of interest

J. S. owns a financial stake in Femtorays Technologies which develops label-free molecular sensors. All other authors declare no conflict of interest.

Data availability

No new data were created or analyzed in this study. Data sharing is not applicable to this article.

Notes and references

1 D. Armani, T. Kippenberg, S. Spillane and K. Vahala, *Nature*, 2003, **421**, 925–928.
2 L. Rayleigh, *Dublin Philosophical Magazine and Journal of Science*, Edinburgh, The London, 1910, vol. 20, pp. 1001–1004.
3 L. Rayleigh, *Dublin Philosophical Magazine and Journal of Science*, Edinburgh, The London, 1914, vol. 27, pp. 100–109.
4 R. D. Richtmyer, *J. Appl. Phys.*, 1939, **10**, 391–398.
5 J. Su, A. F. Goldberg and B. M. Stoltz, *Light Sci. Appl.*, 2016, **5**, e16001.
6 L. Chen, C. Li, Y. Liu, J. Su and E. McLeod, *Sensors*, 2020, **20**, 5420.
7 T. J. Kippenberg, S. M. Spillane and K. J. Vahala, *Opt. Lett.*, 2002, **27**, 1669.
8 K. A. Knapper, K. D. Heylman, E. H. Horak and R. H. Goldsmith, *Adv. Mater.*, 2016, **28**, 2945–2950.
9 W. Bogaerts, P. De Heyn, T. Van Vaerenbergh, K. De Vos, S. Kumar Selvaraja, T. Claes, P. Dumon, P. Bienstman, D. Van Thourhout and R. Baets, *Laser Photonics Rev.*, 2012, **6**, 47–73.
10 M. Soltani, S. Yegnanarayanan and A. Adibi, *Opt. Express*, 2007, **15**, 4694–4704.
11 S. M. Grist, S. A. Schmidt, J. Flueckiger, V. Donzella, W. Shi, S. Talebi Fard, J. T. Kirk, D. M. Ratner, K. C. Cheung and L. Chrostowski, *Opt. Express*, 2013, **21**, 7994.
12 T.-T. J. Su, PhD thesis, California Institute of Technology, 2014.
13 J. Su, *J. Visualized Exp.*, 2015, 53180.
14 T.-T. J. Su, US9739770B2, 2017.
15 T.-T. J. Su, US10309960B2, 2019.
16 *Science*, 2011, **334**, 1496.
17 A. Gin, P.-D. Nguyen, J. E. Melzer, C. Li, H. Strzelinski, S. B. Liggett and J. Su, *Nat. Commun.*, 2024, **15**, 7445.
18 S. Hao, B. Guthrie, S.-K. Kim, S. Balanda, J. Kubicek, B. Murtaza, N. A. Khan, P. Khakbaz, J. Su and W. A. GoddardIII, *Commun. Chem.*, 2024, **7**, 236.
19 A. Gin, P.-D. Nguyen, G. Serrano, G. E. Alexander and J. Su, *npj Biosens.*, 2024, **1**, 9.
20 J. Su, *ACS Photonics*, 2015, **2**, 1241–1245.
21 S.-K. Kim, S. Suebka, A. Gin, P.-D. Nguyen, Y. Tang, J. Su and W. A. GoddardIII, *ACS Pharmacol. Transl. Sci.*, 2024, **7**, 348–362.
22 Y. Wu, Y. Cao, L. Chen, X. Lai, S. Zhang and S. Wang, *Biol. Proced. Online*, 2024, **26**, 15.
23 E. Ozgur, K. E. Roberts, E. O. Ozgur, A. N. Gin, J. R. Bankhead, Z. Wang and J. Su, *Anal. Chem.*, 2019, **91**, 11872–11878.
24 T. Lu, T.-T. J. Su, K. J. Vahala and S. E. Fraser, US8593638B2, 2013.
25 C. Li, T. Lohrey, P.-D. Nguyen, Z. Min, Y. Tang, C. Ge, Z. P. Sercel, E. McLeod, B. M. Stoltz and J. Su, *ACS Appl. Mater. Interfaces*, 2022, **14**, 42430–42440.
26 Y. Xu, A. M. Stanko, C. S. Cerione, T. D. Lohrey, E. McLeod, B. M. Stoltz and J. Su, *ACS Appl. Mater. Interfaces*, 2024, **16**, 5120–5128.
27 S. M. Spillane, T. J. Kippenberg, K. J. Vahala, K. W. Goh, E. Wilcut and H. J. Kimble, *Phys. Rev. A*, 2005, **71**, 013817.
28 C. Li, L. Chen, E. McLeod and J. Su, *Photonics Res.*, 2019, **7**, 939–947.
29 G. Choi and J. Su, *J. Phys.: Photonics*, 2022, **5**, 014001.
30 G. Choi, A. Gin and J. Su, *Opt. Express*, 2022, **30**, 8690–8699.
31 T. J. A. Kippenberg, *Nonlinear optics in ultra-high-Q whispering-gallery optical microcavities*, PhD thesis, California Institute of Technology, 2004.
32 S. Suebka, PhD thesis, The University of Arizona, 2024.
33 J. Su, *Sensors*, 2017, **17**, 540.
34 L. Novotny and B. Hecht, *Principles of Nano-Optics*, Cambridge University Press, Cambridge, 2012.
35 K. Padmaraju, D. F. Logan, T. Shiraishi, J. J. Ackert, A. P. Knights and K. Bergman, *J. Light Technol.*, 2013, **32**, 505–512.
36 T. Carmon, T. J. Kippenberg, L. Yang, H. Rokhsari, S. Spillane and K. J. Vahala, *Opt. Express*, 2005, **13**, 3558.
37 E. D. Black, *Am. J. Phys.*, 2001, **69**, 79–87.
38 W. Weng, J. D. Anstie and A. N. Luiten, *Phys. Rev. Appl.*, 2015, **3**, 044015.
39 S. Hao and J. Su, *Rep. Prog. Phys.*, 2024, **88**, 016402.
40 S. Suebka, A. Gin and J. Su, *Nat. Protoc.*, 2025, 1–35.
41 S. Sang, Y. Wang, Q. Feng, Y. Wei, J. Ji and W. Zhang, *Crit. Rev. Biotechnol.*, 2015, 1–17.
42 J. Meja-Salazar and O. N. OliveiraJr, *Chem. Rev.*, 2018, **118**, 10617–10625.
43 S. Hao and J. Su, *J. Light Technol.*, 2020, **38**, 6393–6401.
44 W. Li, J. Li, L. Wang, Y. Wang, Z. Zhang, S. Liu, B. Gong, Y. Wang and L. Wang, *Nano Lett.*, 2025, **25**, 1706–1714.
45 J. Li, Y. Wang, L. Wang, Y. Wang, Z. Zhang, S. Liu and L. Wang, *ACS Mater. Lett.*, 2025, **7**, 2476–2481.
46 G. T. Luu, C. Ge, Y. Tang, K. Li, S. M. Cologna, A. K. Godwin, J. E. Burdette, J. Su and L. M. Sanchez, *Mol. Cell. Proteomics*, 2023, **22**, 100590.

Published on 11 August 2025. Downloaded on 9/5/2025 5:21:07 PM.

47 J. W. Kerssemakers, E. Laura Munteanu, L. Laan, T. L. Noetzel, M. E. Janson and M. Dogterom, *Nature*, 2006, **442**, 709–712.
48 K. Duy Mac and J. Su, *npj Biosens.*, 2025, **2**, 20.
49 Q. Liu, Y. Ouyang, Y. Wang, S. Zhou, Y. Zhan and L. Wang, *Adv. Healthcare Mater.*, 2025, **14**, 2405058.
50 M. Young Yang, K. Duy Mac, H. R. Strzelinski, S. A. Hoffman, D. Kim, S.-K. Kim, J. Su, S. B. Liggett and W. A. Goddard, *Proc. Natl. Acad. Sci. U. S. A.*, 2024, **121**, e2409987121.
51 J. Su, *ACS Photonics*, 2016, **3**, 718.
52 F. Dell'Olio, J. Su, T. Huser, V. Sottile, L. E. Cortés-Hernández and C. Alix-Panabières, *Laser Photonics Rev.*, 2021, **15**, 2000255.
53 S. Suebka, P.-D. Nguyen, A. Gin and J. Su, *ACS Sens.*, 2021, **6**, 2700–2708.
54 K. Glosz, A. Stolarczyk and T. Jarosz, *Int. J. Mol. Sci.*, 2020, **21**, 6387.
55 G. Chen, T. M. Paronyan, E. M. Pigos and A. R. Harutyunyan, *Sci. Rep.*, 2012, **2**, 343.
56 G. Chen, T. M. Paronyan and A. R. Harutyunyan, *Appl. Phys. Lett.*, 2012, **101**, 053119.
57 O. Tsymbalenko, S. Lee, Y.-M. Lee, Y.-S. Nam, B. C. Kim, J. Y. Kim and K.-B. Lee, *Microchim. Acta*, 2023, **190**, 134.
58 L. Camilli and M. Passacantando, *Chemosensors*, 2018, **6**, 62.
59 T. J. Kippenberg, R. Holzwarth and S. A. Diddams, *Science*, 2011, **332**, 555–559.
60 K. D. Heylman, K. A. Knapper, E. H. Horak, M. T. Rea, S. K. Vanga and R. H. Goldsmith, *Adv. Mater.*, 2017, **29**, 1700037.
61 T. Carmon, L. Yang and K. J. Vahala, *Opt. Express*, 2004, **12**, 4742–4750.
62 T. Voumard, T. Wildi, V. Brasch, R. G. Álvarez, G. V. Ogando and T. Herr, *Opt. Lett.*, 2020, **45**, 6583.
63 R.-K. Shiu, Y.-W. Chen, P.-C. Peng, J. Chiu, Q. Zhou, T.-L. Chang, S. Shen, J.-W. Li and G.-K. Chang, *J. Light Technol.*, 2020, **38**, 5302–5310.
64 H. Liu, Y. Du, X. Li, X. Ji and Y. Su, *ACS Photonics*, 2024, **11**, 5195–5204.
65 Q. Liang, Y.-C. Chan, J. Toscano, K. K. Bjorkman, L. A. Leinwand, R. Parker, E. S. Nozik, D. J. Nesbitt and J. Ye, *J. Breath Res.*, 2023, **17**, 036001.
66 B.-B. Li, Q.-Y. Wang, X.-F. Jiang, Q. Gong and Y.-F. Xiao, *Photonic Sens.*, 2011, 80340J.
67 J. Su, A. F. Goldberg and B. M. Stoltz, *Light: Sci. Appl.*, 2016, **5**, e16001.
68 K. D. Heylman, N. Thakkar, E. H. Horak, S. C. Quillin, C. Cherqui, K. A. Knapper, D. J. Masiello and R. H. Goldsmith, *Nat. Photonics*, 2016, **10**, 788–795.
69 S. Hao, S. Suebka and J. Su, *Light: Sci. Appl.*, 2024, **13**, 195.
70 T. Tomimatsu, J. Miyazaki, Y. Kano and T. Kobayashi, *Biomed. Opt. Express*, 2017, **8**, 2965–2975.
71 J. Miyazaki and Y. Toumon, *Biomed. Opt. Express*, 2019, **10**, 5852–5861.
72 J. W. Lichtman and J.-A. Conchello, *Nat. Methods*, 2005, **2**, 910–919.
73 P.-D. Nguyen, X. Zhang and J. Su, *ACS Appl. Nano Mater.*, 2019, **2**, 7839–7847.
74 M. D. Baaske, M. R. Foreman and F. Vollmer, *Nat. Nanotechnol.*, 2014, **9**, 933–939.
75 R. Waldron, *Proc. IEE Part C*, 1960, **107**, 272–274.
76 J. E. Melzer and E. McLeod, *ACS Nano*, 2018, **12**, 2440–2447.
77 G. Pesce, P. H. Jones, O. M. Maragò and G. Volpe, *Eur. Phys. J. Plus*, 2020, **135**, 949.
78 K. V. Serebrennikova, A. N. Berlina, D. V. Sotnikov, A. V. Zherdev and B. B. Dzantiev, *Biosensors*, 2021, **11**, 512.
79 L. Chen, C. Li, Y.-M. Liu, J. Su and E. McLeod, *Photon. Res.*, 2019, **7**, 967–976.
80 S. Suebka, E. McLeod and J. Su, *Light: Sci. Appl.*, 2024, **13**, 75.
81 B.-B. Li, Y.-F. Xiao, C.-L. Zou, Y.-C. Liu, X.-F. Jiang, Y.-L. Chen, Y. Li and Q. Gong, *Appl. Phys. Lett.*, 2011, **98**, 021116.
82 A. R. Anwar, M. Mur and M. Humar, *ACS Photonics*, 2023, **10**, 1202–1224.
83 J. Wu, X. Guo, A. P. Zhang and H.-Y. Tam, *Opt. Express*, 2015, **23**, 29708–29714.
84 X. Hao and J. Ke, Temporal multiplexing coding strategy for spatiotemporal compressed imaging, *Fourth International Computational Imaging Conference (CITA 2024)*, SPIE, 2025, vol. 13542, DOI: **10.1117/12.3057330**.

 This journal is © The Royal Society of Chemistry 2025